Journal of King Saud University - Science 36 (2024) 103058

Contents lists available at ScienceDirect

Journal of King Saud University - Science

journal homepage: www.sciencedirect.com

Full Length Article

Invisible dark matter decays of a non-Standard Model like CP-even scalar boson

Maien Binjonaid

Department of Physics and Astronomy, King Saud University, Riyadh, Saudi Arabia

ARTICLE INFO

Keywords:
Keywords singlet extensions
Extended Higgs sectors
BSM phenomenology
Dark matter phenomenology
Supersymmetric models
Non-supersymmetric models
Collider phenomenology
LHC phenomenology
Invisible decays
non-SM Higgs decay

ABSTRACT

We investigate two extensions of the standard model that include particle dark matter candidates: the Next-to-Two Higgs Doublet Model and the Next-to-minimal Supersymmetric Standard Model. These models feature a non-Standard Model like CP-even scalar with a sub-TeV mass, denoted by H_2, among other particles. At a 13 TeV proton–proton collider, the primary production channel for such scalars is via the fusion of a pair of gluons. Subsequently, these scalars can decay invisibly into a pair of dark matter candidates, which can be dominant. In the supersymmetric model, it is possible for the Lightest Supersymmetric Particle (LSP) and Next-to Lightest Supersymmetric Particle (NLSP) to be mass degenerate, leading to quasi-invisible H_2 decays to LSP+NLSP and NLSP+NLSP. We present the predictions of both models for this challenging scenario while ensuring compatibility with recent experimental constraints.

1. Introduction

The discovery of the Standard Model (SM) like Higgs boson at the Large Hadron Collider (LHC) (Aad et al., 2012; Chatrchyan et al., 2012) marked the completion of the SM of particle physics, and opened the door for what could lay beyond it, which is usually called Beyond the SM (BSM) phenomenology. The SM suffers from multiple shortcomings, such as lacking a Dark Matter (DM) candidate, the issue of neutrino mass, the lightness of the Higgs mass (the hierarchy problem), and other issues. The limitations of the SM motivate the construction of several extensions. For instance, a well-known extension is the Minimal-Supersymmetric Standard Model (MSSM), which solves the hierarchy problem and provides a DM candidate. However, given the absence of supersymmetry (SUSY) at collider searches, it is possible to consider a case where most SUSY particles reside at high scales beyond the reach of current experiments. What remains could include the extended Higgs sector of such models. A general non-SUSY version would be the well-known Two-Higgs-Doublet Model (2HDM), which allows for broader Higgs sector structures and Yukawa couplings.

However, both the 2HDM and the MSSM have their own issues. The 2HDM, in its simplest form, where both Higgs doublets acquire Vacuum Expectation Values (VEVs) does not contain a DM candidate. As for the MSSM, it contains a SUSY Higgs/Higgsino mass term μ that respects all symmetry conditions, but it is unclear at which scale it is generated, which is known in the literature as the "μ-problem". Solving the latter issue leads us naturally to the Next-to-Minimal Supersymmetric Model (NMSSM), which features an additional SM singlet. A non-SUSY version of such a model is the Next-to −2-Higgs Higgs Doublet Model (N2HDM). Both models are subject to intensive research as they provide DM candidates and novel phenomenology relevant to LHC and DM searches.

The Higgs sectors of the N2HDM and NMSSM comprise an SM-like Higgs (h), CP-even and odd neutral scalars ($H_1, H_2, H_3/A_1, A_2$), and charged Higgses ($H^{\pm}$). comprehensive reviews of both models are given in Mühlleitner et al. (2017a) and Ellwanger et al. (2010). In these models, the DM particle can be an SM singlet. Furthermore, it is possible for the non-SM Higgs bosons to decay invisibly to DM, making them difficult to detect if such decays are dominant. Hence, understanding the size and dominance of these decays in different parameter regions could be relevant for LHC searches.

A number of papers considered different types of the N2HDM with either real or complex singlets. For instance, the effects of the mixing between the doublets and a singlet with $\langle s \rangle \neq 0$ are studied in Chen et al. (2014), while in Drozd et al. (2014) the model, with a DM candidate, was confronted with relevant experimental constraints at the time. Comparing the cases with a real and complex singlet added to the 2HDM is provided in Dutta et al. (2022), and it was noted that the case with a real singlet provides larger values of the dark matter relic abundance (Ωh^2) throughout the parameter space.

On the other hand, the NMSSM is a much richer model given the number of new SUSY particles and its connection to the Grand Unification (GUT) scale. The phenomenology of the Higgs sector in different

E-mail address: maien@ksu.edu.sa.

https://doi.org/10.1016/j.jksus.2023.103058
Received 1 May 2023; Received in revised form 30 November 2023; Accepted 8 December 2023
Available online 9 December 2023

variants of the NMSSM is considered in e.g. Miller et al. (2004), Wang and Zhu (2020b), Baum et al. (2019), King et al. (2014), Ellwanger and Hugonie (2012), Telba and Binjonaid (2021a,b). Different types of DM candidates, including the case with singlet DM, are considered in e.g. Wang and Zhu (2020a), Domingo et al. (2022), Cao et al. (2023), Ellwanger and Teixeira (2014), Adhikary et al. (2023). The case where the DM is singlino-like requires a specific setup in which the parameters λ and κ and the ratio κ/λ are quite small. In this work, we do not specifically target this scenario, as we are allowing λ and κ to be as large as possible. It is known in the NMSSM that a large value of λ enhances the tree-level mass of the SM-Higgs boson, although it still needs to be below 0.7 to abide by GUT scale perturbativity.

From a phenomenological point of view, it is crucial to analyze the differences between models. Indeed comparing some aspects of the N2HDM with the NMSSM was performed in different studies. For example, Mühlleitner et al. (2017b), Azevedo et al. (2019) show that it is possible to use the couplings sums of the Higgs boson to VV and $f\bar{f}$ to distinguish these models at the LHC, and that future e^+e^- colliders can be used to do so by setting limits on the possible singlet or pseudoscalar admixtures to the SM Higgs. The possibility of explaining certain anomalies in the LHC data using the N2HDM and the NMSSM is considered in Biekötter et al. (2022).

As mentioned earlier, the additional non-SM CP-even scalar field H_2 could have dominant decays into DM, hence making the task of observing it very challenging. Within the context of the MSSM, Ananthanarayan et al. (2015) investigates invisible decays of H_2. The analysis includes the case where H_2 decays into the Lightest Supersymmetric Particle (LSP), which is the DM particle, and Next-to LSP (NLSP) with degenerate mass. Such decays are called "quasi-invisible". For the specific parameter space, it was found that $Br(H_2 \to \tilde{\chi}_1\tilde{\chi}_1)$ is 16% at most. As for the NMSSM, and as far as we know, no dedicated analysis was performed for such cases, nor a comparison to the N2HDM was made.

We fill this gap, limiting our analysis to the second lightest CP-even non-SM-like Higgs (H_2). Firstly, we will ask what are the maximum branching ratios of H_2 into DM given the latest experimental constraints. Second, we study the production of H_2 via gluon fusion at a 13 TeV pp collider and calculate the cross-section times the branching ratio. The paper is organized as follows. In Section 2, we present a general overview of the two considered models, their input parameters, Higgs sectors, and relevant quantities. Next, Section 3 details the tools utilized in this paper and the constraints applied in analyzing the parameter space of each model. In Section 4, the results for both models are presented. And finally, the discussion and conclusions are given in Section 5.

2. The models

2.1. Overview of the N2HDM

The N2HDM comprises two-Higgs-doublets (Φ_1 and Φ_2) and a real singlet (Φ_S), and its potential reads (following the conventions in Mühlleitner et al. (2017a)),

$$\begin{aligned} V &= m_{11}^2|\Phi_1|^2 + m_{22}^2|\Phi_2|^2 - m_{12}^2(\Phi_1^\dagger\Phi_2 + h.c.) + \frac{\lambda_1}{2}(\Phi_1^\dagger\Phi_1)^2 + \frac{\lambda_2}{2}(\Phi_2^\dagger\Phi_2)^2 \\ &+ \lambda_3(\Phi_1^\dagger\Phi_1)(\Phi_2^\dagger\Phi_2) + \lambda_4(\Phi_1^\dagger\Phi_2)(\Phi_2^\dagger\Phi_1) + \frac{\lambda_5}{2}[(\Phi_1^\dagger\Phi_2)^2 + h.c.] \\ &+ \frac{1}{2}m_S^2\Phi_S^2 + \frac{\lambda_6}{8}\Phi_S^4 + \frac{\lambda_7}{2}(\Phi_1^\dagger\Phi_1)\Phi_S^2 + \frac{\lambda_8}{2}(\Phi_2^\dagger\Phi_2)\Phi_S^2\,, \end{aligned} \tag{1}$$

where the mass parameters m_{ij} ($i,j = 1,2$ and $i \le j$) correspond to the doublets, while m_S is the mass parameter of the singlet, and the λ's are quartic couplings between the scalar fields. Moreover, the structure of the potential in Eq. (1) respects two discrete symmetries. The first is a $\mathbb{Z}_2$ symmetry similar to that in the 2HDM, under which Φ_1 and Φ_S are even, while Φ_2 is odd. The second is a new $\mathbb{Z}_2'$ symmetry, under which Φ_1 and Φ_2 are even, while Φ_S is odd. This $\mathbb{Z}_2'$ symmetry is responsible for the existence of a dark matter candidate in the theory if Φ_S does not acquire a VEV.

For the case where the $\mathbb{Z}_2'$ symmetry is intact, only the Higgs doublets acquire VEVs. This case is named "the Dark Singlet Phase (DPS)" by the authors of Mühlleitner et al. (2017a), and is the one we are considering (we will denote the model in the subsequent sections by DSP-N2HDM). Moreover, the vacuum structure is,

$$\langle\Phi_1\rangle = \frac{1}{\sqrt{2}}\begin{pmatrix}0\\ v_1\end{pmatrix}, \qquad \langle\Phi_2\rangle = \frac{1}{\sqrt{2}}\begin{pmatrix}0\\ v_2\end{pmatrix}, \qquad \langle\Phi_S\rangle = 0\,, \tag{2}$$

where $v_1 \equiv v\cos\beta$, and $v_2 \equiv v\sin\beta$, while $\tan\beta \equiv \frac{v_2}{v_1}$, and $v = \sqrt{v_1^2 + v_2^2}$. The gauge eigenstates are rotated into mass eigenstates via a rotation matrix $\mathcal{R}$ that depends on the rotation angle α. The rotation is done such that $m_{H_1} \le m_{H_2}$. On the other hand, the dark singlet scalar is $H_3 \equiv H_D$, as it does not mix with the other Higgs scalars.

The couplings of H_1 and H_2 to SM particles are the same as in Type-I 2HDM. For H_2, which is our focus in this paper, $c(H_2\bar{f}f) = \sin\alpha/\sin\beta$, while $c(H_2VV) = \cos(\alpha-\beta)$. In addition to these couplings, we have the triple-Higgs couplings that are responsible for the possible decays of the CP-even Higgs scalars into DM. Particularly,

$$g(H_2H_DH_D) = \lambda_7 v\cos\beta\cos\alpha + \lambda_8 v\sin\beta\sin\alpha \tag{3}$$

Finally, the DSP-N2HDM is represented by 11 input parameters,

$$v\,,\quad \tan\beta\,,\quad m_{H_1}\,,\quad m_{H_2}\,,\quad m_{H_D}\,,\quad m_A\,,\quad m_{H^\pm}\,,\alpha\,,\quad \lambda_6\,,\quad \lambda_7\,,\quad \lambda_8\,,$$

where m_{H_1} is taken to be the mass of the SM Higgs boson, while m_{H_D} is the mass of the DM candidate, m_A is the mass of the CP-odd Higgs boson, $m_{H^\pm}$ is the mass of the charged Higgs bosons. The other parameters were defined earlier.

2.2. Overview of the NMSSM

The NMSSM is a well-known SUSY model that solves the $\mu-$problem in the MSSM due to adding a singlet superfield S. This singlet couples to the Higgs doublets, extending the well-known MSSM superpotential. Following the convention in Ellwanger et al. (2010), the superpotential is,

$$\begin{aligned} W_{NMSSM} &= h_u\hat{Q}.\hat{H}_u\hat{U}_R^c + h_d\hat{H}_d.\hat{Q}\hat{D}_R^c + h_e\hat{H}_d.\hat{L}\hat{E}_R^c \\ &+ \lambda\hat{S}\hat{H}_u.\hat{H}_d + \frac{1}{3}\kappa\hat{S}^3. \end{aligned} \tag{4}$$

where $\hat{Q}$ and $\hat{L}$ are left-handed doublet quark and lepton superfields, whereas $\hat{U}$, $\hat{D}$ and $\hat{E}$ are right-handed singlet up-type quark, down-type quark, and lepton superfields. Unlike the N2HDM, the NMSSM singlet superfield obtains a VEV $\langle S\rangle = s$. To avoid a massless Axion at the weak scale, the last term is introduced (Peccei and Quinn, 1977b,a).

Furthermore, the soft SUSY breaking lagrangian of the NMSSM is,

$$\begin{aligned} -\mathcal{L}_{soft} &= m_{H_u}^2\left|H_u\right|^2 + m_{H_d}^2\left|H_d\right|^2 + m_S^2\left|S\right|^2 + m_Q^2\left|Q^2\right| \\ &+ m_U^2\left|U_R^2\right| + m_D^2\left|D_R^2\right| + m_L^2\left|L^2\right| + m_E^2\left|E_R^2\right| \\ &+ \frac{1}{2}\begin{bmatrix} M_1\lambda_1\lambda_1 + M_2\sum_{i=1}^{3}\lambda_2^i\lambda_{i2} \\ +M_3\sum_{a=1}^{8}\lambda_3^a\lambda_{a3}\end{bmatrix} \\ &+ h_uA_uQ\cdot H_uU_R^2 - h_dA_dQ\cdot H_dD_R^2 - h_eA_eL\cdot H_dE_R^2 \\ &+ \lambda A_\lambda H_u\cdot H_dS + \frac{1}{3}\kappa A_\kappa S^3 + h.c. \end{aligned} \tag{5}$$

which comprises terms for scalar mass parameters, gaugino mass parameters, trilinear couplings, and dimensionless couplings.

The non-SM CP-even Higgs couplings to two neutralinos (with a focus on the NLSP and the LSP) is,

$$\begin{aligned} H_2\chi_i^0\chi_j^0 :\ &\frac{\lambda}{\sqrt{2}}(S_{21}\Pi_{ij}^{45} + S_{22}\Pi_{ij}^{35} + S_{23}\Pi_{ij}^{34}) - \sqrt{2}\kappa S_{23}N_{i5}N_{j5} \\ &+ \frac{g_1}{2}(S_{21}\Pi_{ij}^{13} - S_{22}\Pi_{ij}^{14}) - \frac{g_2}{2}(S_{21}\Pi_{ij}^{23} - S_{22}\Pi_{ij}^{24}). \end{aligned} \tag{6}$$

where S_{ij} represent elements of the Higgs mixing matrix, and $\Pi_{ij}^{ab} \equiv N_{ia}N_{jb} + N_{ib}N_{ja}$ are defined in terms of the mixing matrices of the neutralinos.

Finally, the input parameters of the NMSSM, which are specified at the GUT scale, are

$$m_0,\ m_{1/2},\ A_0,\ A_\lambda,\ A_\kappa,\ \lambda,\ \kappa,\ \tan\beta,\ \mu_{\text{eff}}.$$

comprising scalar and gaugino mass parameters, trilinear couplings, the singlet-Higgs coupling λ, the cubic singlet self-coupling κ, and $\mu_{\text{eff}} \equiv \lambda s$. Both m_{H_u} and m_{H_d} can have the same value as m_0 at the GUT scale, but the case where they differ from m_0 is called the Non-Universal Higgs NMSSM (NUH-NMSSM), which we consider here. However, due to the nature of the tool we use (described in Section 3) these two parameters are computed.

3. The parameter spaces

3.1. The DSP-N2HDM

To generate the mass-spectrum generator of the N2HDM we use `N2HDECAY` (Engeln et al., 2019), and is embedded in the state-of-the-art scanning tool `ScannerS` (Mühlleitner et al., 2022). Specifically, we consider the dark-singlet phase of the N2HDM and scan the parameter space over the following ranges:

$$\begin{aligned} m_{H_2} &= [10-1500]\ \text{GeV}, & m_{H_D} &= [1-1500]\ \text{GeV},\\ m_A &= [1-1500]\ \text{GeV}, & m_{H^\pm} &= [150-1500]\ \text{GeV},\\ \alpha &= [-1.5-1.6], & \tan\beta &= [0.8-25],\\ m_{12}^2 &= [1\times10^{-3} - 5\times10^5]\ \text{GeV}^2, & & \\ \lambda_6 &= [0-20], & \lambda_{7,8} &= [-30-30]. \end{aligned}$$

The package applies stringent theoretical and experimental constraints on the model. The former includes perturbative unitarity, boundedness, vacuum stability, constraints from electroweak precision, and flavor conservation. The latter include Higgs searches and measurements via interfacing with `HiggsBounds` (v.5.9) (Bechtle et al., 2020) and `HiggsSignals` (v.2.6) (Bechtle et al., 2021), and Dark matter constraints using `MicrOMEGAs` (v.5) (Belanger et al., 2021). It is worth mentioning that HiggsBounds provides the production cross-section of H_2 via gluon fusion at 13 TeV via tabulated results from `SusHi1.6.1` (Harlander et al., 2017).

3.2. The NUH-NMSSM

The parameter space of the NMSSM was scanned using `NMSSMTools` (v.5.6) (Ellwanger et al., 0000, 2005; Ellwanger and Hugonie, 2006; Das et al., 2012). A combination of random and Markov Chain Monte Carlo (MCMC) sampling methods was deployed. The scanned ranges of the input parameters are:

$$\begin{aligned} m_0 &= [1-4000]\ \text{GeV}, & m_{1/2} &= [1-4000]\ \text{GeV},\\ A_0, A_\lambda, A_\kappa &= [-3000-3000]\ \text{GeV}, & \tan\beta &= [1-30]\\ \lambda, \kappa &= [0.01-0.7], & \mu_{eff} &= [100-1500]\ \text{GeV}. \end{aligned}$$

As mentioned in Section 2.2, the parameters m_{H_u} and m_{H_d} are computed, and hence what we are considering here is the NUH-NMSSM. The constraints implemented in `NMSSMTools` are similar to those in `ScannerS` if not more comprehensive (see the tool's History Section for all constraints included and the corresponding references). These include non-tachyonic masses, successful Electroweak Symmetry Breaking, and the existence of a global minimum, which represents the theoretical constraints. In contrast, the phenomenological ones include: Flavor physics, LHC constraints on sparticles, satisfying the upper limit on dark matter relic density using `MicrOMEGAs` (v.5). As for the SM-Higgs couplings, we consider recent results from the LHC, and select points to be within 3σ away from the central values of the combination of ATLAS and CMS results (Tumasyan et al., 2022; ATLAS Collaboration, 2022), which makes our results subject to the latest LHC limits. Finally, the production cross-section of H_2 via gluon fusion is calculated through the method described in Ellwanger and Hugonie (2022), where the data for the BSM production cross-section at 13 TeV is obtained from CERN Yellow Report (0000) and subsequently multiplied by the relevant reduced coupling squared. Thus, the calculation accounts for a significant portion of the radiative Quantum Chromodynamics corrections, leaving theoretical uncertainties of the order of $O(10\%)$.

4. Results

4.1. The DSP-N2HDM

The results of the N2HDM with a singlet dark matter are shown in Figures 1.a. to 1.e. We have restricted our analysis to points where $m_{H_2} \leq 1000$ GeV, for which a total of 20k successful points are collected. Fig. 1.a. shows a scatter plot of the branching ratio of H_2 to a pair of dark matter particles ($Br(H_2 \to H_D H_D)$) versus m_{H_2}. The color indicates the dark matter mass, m_{H_D}. As can be seen, m_{H_2} ranges from 222 GeV to 1000 GeV, while m_{H_D} ranges from 100 GeV to 497 GeV. The branching ratio $Br(H_2 \to H_D H_D)$ can reach values close to one, especially for regions where the mass of the dark singlet is below 200 GeV. As the mass increases, the branching ratio reduces significantly, as seen in the plot's red corner. A representative point where $Br(H_2 \to H_D H_D) \sim 1$ corresponds to the parameter space point: $m_{H_2} = 337$ GeV, $m_{H_D} = 127$ GeV, $\tan\beta = 3$, $\sigma(gg \to H_2) = 1.1$ pb, and $\Omega h^2 = O(10^{-9})$.

Next, Fig. 1.b. displays the production of H_2 via gluon fusion ($\sigma(gg \to H_2)$) versus m_{H_2}. It ranges from 3×10^{-6} pb to 5.8 pb. The maximum value occurs at $m_{H_2} = 378$ GeV, $m_{H_D} = 170$ GeV, $\tan\beta = 1.5$, $Br(H_2 \to H_D H_D) = 0.95$, and $\Omega h^2 = O(10^{-8})$. The dependence on $\tan\beta$ is shown in Fig. 1.c. First, in the allowed regions, $\tan\beta$ takes values between 0.9 and 28. We note that most successful points lie in regions where $\tan\beta < 5$. The distribution of the branching ratio to dark matter appears to be nearly uniform. However, smaller values of $\tan\beta$ tend to be associated with branching ratio below 0.1. As $\tan\beta$ slightly increases from 0.9 to 1.5, the branching ratio exceeds 0.6.

Fig. 1.d. shows the branching ratio times the cross-section. The values range between $O(10^{-12})$ pb and 5.6 pb. Moreover, for a given mass of m_{H_2}, the maximum value of $Br \times \sigma$ slightly decreases with the increase of m_{H_2}. The maximum value of $Br \times \sigma$ found in the allowed parameter space is achieved at $m_{H_2} = 378$ GeV, $m_{H_D} = 170$ GeV, $\tan\beta = 1.5$, $Br(H_2 \to H_D H_D) = 0.95$, and $\Omega h^2 = O(10^{-8})$. At this point, H_2 mainly decays into $t\bar{t}$ with a percentage of 3%, followed by $h_1 h_1$ at 0.5% and W^+W^- at 0.4%.

Finally, we note that the relic density in the scanned parameter space is almost always below the lower Planck bound, as shown in Fig. 1.e. Hence, while this parameter space provides a candidate for dark matter, it cannot explain all dark matter phenomena. A representative point where the relic density is fully explained by this model corresponds to $m_{H_2} = 914$ GeV, $m_{H_D} = 180$ GeV, $\tan\beta = 1.4$, $Br(H_2 \to H_D H_D) \approx 0.11$, $\sigma(gg \to H_2) \approx 0.11$ pb and $\Omega h^2 \approx 0.11$. In this case, the dominant decay of H_2 is to $t\bar{t}$ pair at 88%.

4.2. The NUH-NMSSM

In this subsection, we present the results for the NMSSM with boundary conditions set at the GUT scale. A total of 120k valid points are collected, and the data corresponds to $m_{H_2} < 1$ TeV. Fig. 2.a shows the results of our scans in the usual m_0-$m_{1/2}$ plane, where the first parameter ranges from ~ 0 to 5961 GeV, while the second ranges between 690 GeV and 10460 GeV. As can be seen in the Figure, values of $m_{H_2} \leq 350$ GeV correspond to portions of the parameter space where $m_{1/2} < 2500$ GeV, while m_0 can take the full range of its allowed values. Regions where $m_{1/2} > 2500$ GeV are associated with $m_{H_2} > 350$ GeV.

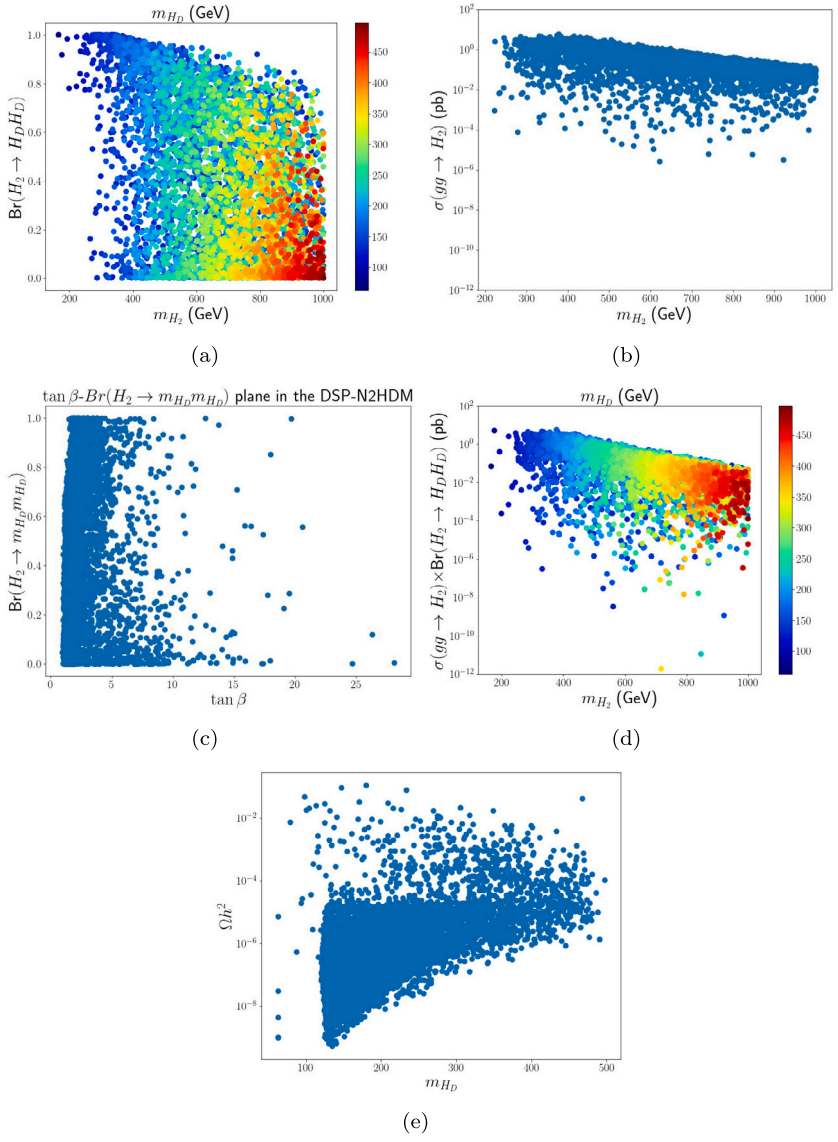

Fig. 1. Two dimensional scatter plots of (a) $Br(H_2 \to H_D H_D)$ versus m_{H_2} with m_{H_D} shown in color (b) $\sigma(gg \to H_2)$ versus m_{H_2} (c) $Br(H_2 \to H_D H_D)$ versus $\tan\beta$ (d) $\sigma \times Br$ versus m_{H_2} with m_{H_D} shown in color (e) The relic density.

The shape of the parameter space reflects the fact that we have used both random scanning method (especially the box where $m_{1/2}, m_0 <$ 2500 GeV) as well as the MCMC method described in Section 3.

As mentioned in Section 1, the main production channel of the neutral scalars is via the fusion of two gluons. The results are displayed in Fig. 2.b where the minimum and the maximum values of the production as a function of m_{H_2} are $\mathcal{O}(10^{-10})$ pb and 2.2 pb, respectively. In the subsequent analysis, we require that $Br(H_2 \to \tilde{\chi}_1 \tilde{\chi}_1) > 0$. By doing so, some points in the parameter space are removed, and what remains is a parameter space where $\sigma^{\max}_{gg \to H_2} \sim 0.51$ pb. This corresponds to $m_{H_2} = 210$ GeV, $m_{\tilde{\chi}_1} = 101$ GeV, and $Br(H_2 \to \tilde{\chi}_1 \tilde{\chi}_1) = 0.012$.

Moving on to the branching ratio, Fig. 2.c depicts the allowed ranges of $Br(H_2 \to \tilde{\chi}_1 \tilde{\chi}_1)$ as a function of m_{H_2} and $m_{\tilde{\chi}_1}$ (indicated by color). The branching ratio takes values ranging from ~ 0 to 0.87. The highest value occurs at $m_{H_2} = 212$ GeV, and $m_{\tilde{\chi}_1} = 98$ GeV. These values correspond to $\tan\beta = 17$, and are associated with $\Omega h^2 \sim 0.01$ and $\sigma_{ggH_2} \sim 0.1$ pb. In this case, H_2 decays to $b\bar{b}$ with Br~ 0.1, and to W^+W^- and $\tau\bar{\tau}$ with Br~ 0.01.

Fig. 2.d shows the dependence of the invisible decay branching ratio on $\tan\beta$, ranging from 1.8 to 30. The maximum value of $Br(H_2 \to \tilde{\chi}_1 \tilde{\chi}_1)$ is obtained only for $\tan\beta > 5$.

Fig. 2.e displays $\sigma(gg \to H_2) \times Br(H_2 \to \tilde{\chi}_1 \tilde{\chi}_1)$. The maximum value is 0.1 pb, which takes place at $m_{H_2} = 216$ GeV, $m_{\tilde{\chi}_1} = 102$ GeV, $\tan\beta = 12$, $\Omega h^2 = 0.001$, $Br \approx 0.3$ and $\sigma \approx 0.3$ pb. In this case, H_2 is more likely to decay into W^+W^-, which accounts for 50% of the decays, while ZZ accounts for 20%.

For completeness, Fig. 2.f shows the relic density as a function of the mass of the DM particle. All points in the parameter space are associated with values below the lower Planck limit, in which case the DM particle is insufficient to account for all of the observed DM relic density.

We turn to the case where $\tilde{\chi}_2$ and $\tilde{\chi}_1$ are mass degenerate. This interesting case can lead to $\tilde{\chi}_2$ being long-lived and hence escaping detection. There are two cases here. The first is when H_2 decays to $\tilde{\chi}_2$ and $\tilde{\chi}_1$, and the second is when it decays to a pair of $\tilde{\chi}_2$. The results for both cases are shown in Fig. 3. Starting with $H_2 \to \tilde{\chi}_2 \tilde{\chi}_1$, we can see in Fig. 3.a that the branching ratio can reach a maximum value of 0.01. Here the most likely decays are to $\tilde{\chi}_1 \tilde{\chi}_1$ at 45%, to $\chi^+\chi^-$ at 40%, to W^+W^- at 6.5%, to $b\bar{b}$ at 3%, to ZZ at 3%, and to $\tilde{\chi}_2 \tilde{\chi}_2$ at 2%. Furthermore, the maximum value of $\sigma \times Br$ is 0.001 pb, which is displayed in Fig. 3.c. This occurs at $m_{H_2} = 456$ GeV, $m_{\tilde{\chi}_1} \approx m_{\tilde{\chi}_2} = 107$ GeV, $\sigma(gg \to H_2) \sim 0.23$ pb, and $Br(H_2 \to \tilde{\chi}_2 \tilde{\chi}_1) \sim 0.003$. The other

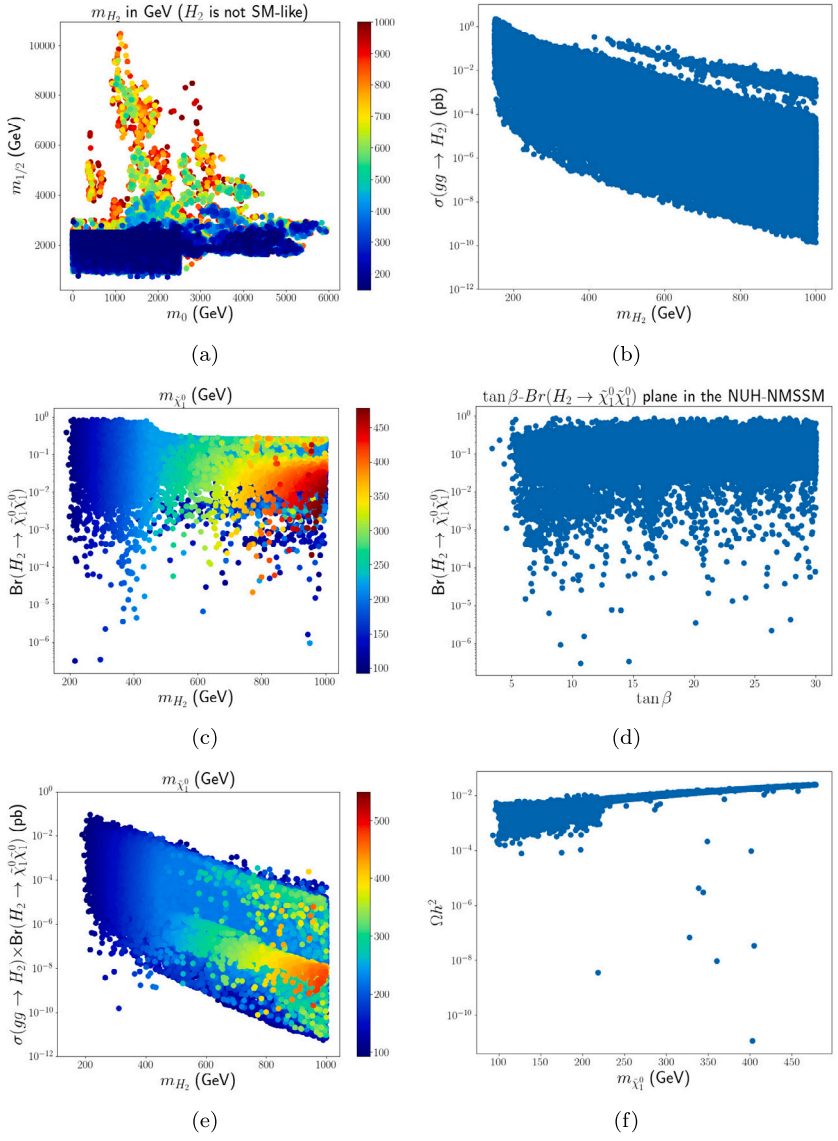

Fig. 2. Two dimensional scatter plots of (a) $m_{1/2}$ versus m_0 (b) $\sigma(gg \to H_2)$ as a function of m_{H_2} (c) $Br(H_2 \to \tilde{\chi}_1\tilde{\chi}_1)$ as a function of m_{H_2} (d) The dependence of Br on $\tan\beta$ (e) $\sigma \times Br$ as a function of m_{H_2} (f) The relic density.

relevant decays of H_2 account for branching ratios of 0.48 to $b\bar{b}$, 0.35 to $t\bar{t}$, 0.065 to $\tau\bar{\tau}$, 0.041 to H_1H_1, and 0.02 to W^+W^- and $\chi^+\chi^-$.

Finally, we consider the second case, displayed in Fig. 3.b. The maximum value of $Br(H_2 \to \tilde{\chi}_2\tilde{\chi}_2)$ is 0.25. while it is 0.5 to $\chi^+\chi^-$, and 0.25 to $\tilde{\chi}_1\tilde{\chi}_1$. And the maximum value of $\sigma \times Br$ is 0.01 pb, which is achieved at $m_{H_2} = 291$ GeV, $m_{\tilde{\chi}_1} \approx m_{\tilde{\chi}_2} = 109$ GeV, $\sigma(gg \to H_2) \sim 0.13$ pb, and $Br(H_2 \to \tilde{\chi}_2\tilde{\chi}_1) \sim 0.1$. Other relevant branching ratios of H_2 are 0.29 to W^+W^-, 0.2 to $\chi^+\chi^-$, 0.18 to H_1H_1, 0.14 to both $\tilde{\chi}_1\tilde{\chi}_1$, and 0.12 to ZZ.

5. Discussion and conclusion

In this paper, we considered the production of a non-SM-like CP-even Higgs boson H_2 via gluon fusion at 13 TeV, and its subsequent decay into DM particle in two well-motivated extensions of the SM, the DSP-N2HDM, and the NUH-NMSSM.

The parameter space of the DSP-N2HDM was scanned subject to recent experimental constraints, including LHC and DM searches. The analysis was restricted to points where $m_{H_2} \leq 1000$ GeV. We found that the branching ratio $Br(H_2 \to H_DH_D)$ can reach values close to one, especially for regions where the mass of the dark singlet is below 200 GeV, which is consistent with previous literature. The production of H_2 via gluon fusion ranges between 3×10^{-6} pb and 5.8 pb, with most successful points having $\tan\beta < 5$. The maximum value of $Br \times \sigma$ found in the allowed parameter space corresponds to $m_{H_2} = 378$ GeV, $m_{H_D} = 170$ GeV, $\tan\beta = 1.5$, $Br(H_2 \to H_DH_D) = 0.95$, and $\Omega h^2 = O(10^{-8})$. We note that the relic density is almost always below the lower bound. Hence, this region of parameter space is insufficient to explain all dark matter phenomena.

On the other hand, the allowed parameter space of the NUH-NMSSM (with $m_{H_2} < 1$ TeV) was also explored under recent experimental limits. The production cross-section at $\sqrt{s} = 13$ TeV was computed, with values ranging from $\mathcal{O}(10^{-10})$ pb to 2.2 pb, and only the points with $Br(H_2 \to \tilde{\chi}_1\tilde{\chi}_1) > 0$ were considered. The allowed range of the branching ratio $Br(H_2 \to \tilde{\chi}_1\tilde{\chi}_1)$ was computed, and it assumes values between ~ 0 to 0.87. The maximum value of the quantity $\sigma(gg \to H_2) \times Br(H_2 \to \tilde{\chi}_1\tilde{\chi}_1)$ was found to be 0.1 pb.

In the case where $\tilde{\chi}_2$ and $\tilde{\chi}_1$ are mass degenerate, there are two cases to consider. Firstly, when H_2 decays to $\tilde{\chi}_2$ and $\tilde{\chi}_1$, the branching ratio can reach a maximum value of 0.01, with the most likely decays being to $\tilde{\chi}_1\tilde{\chi}_1$ and $\chi^+\chi^-$. The maximum value of $\sigma \times Br$ is 0.001 pb, occurring when $m_{H_2} = 456$ GeV, $m_{\tilde{\chi}_1} \approx m_{\tilde{\chi}_2} = 107$ GeV, $\sigma(gg \to H_2) \sim 0.23$ pb,

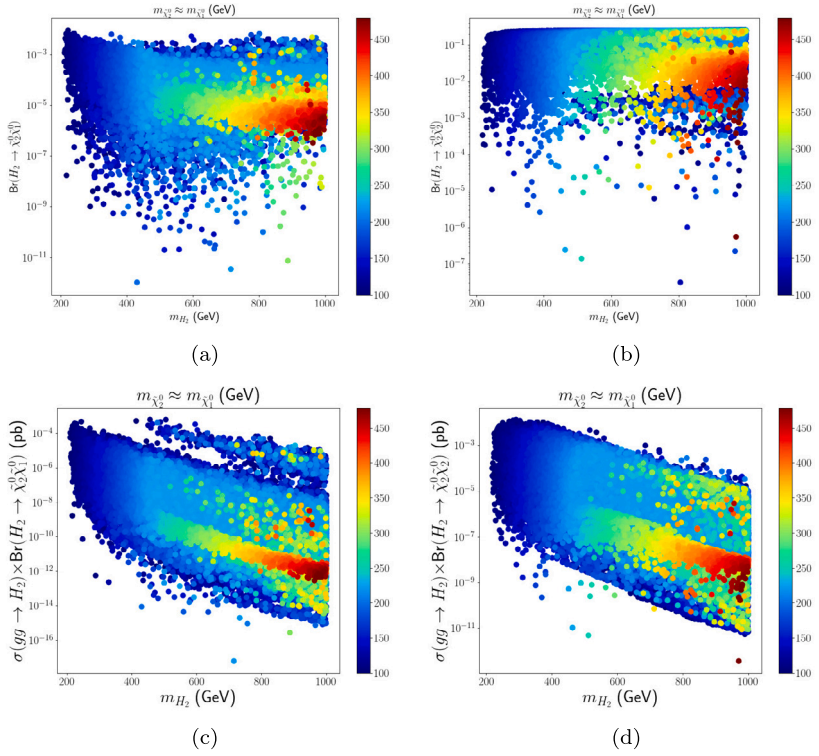

Fig. 3. Two dimensional scatter plots of (a) $Br(H_2 \to \tilde{\chi}_2\tilde{\chi}_1)$ versus m_{H_2} (b) $Br(H_2 \to \tilde{\chi}_2\tilde{\chi}_2)$ versus m_{H_2} (c) $\sigma \times Br(H_2 \to \tilde{\chi}_2\tilde{\chi}_1)$ versus m_{H_2} (d) $\sigma \times Br(H_2 \to \tilde{\chi}_2\tilde{\chi}_2)$ versus m_{H_2}.

and $Br(H_2 \to \tilde{\chi}_2\tilde{\chi}_1) \sim 0.003$. The second case is when H_2 decays to a pair of $\tilde{\chi}_2$, with a maximum branching ratio of 0.25 to $\tilde{\chi}_2\tilde{\chi}_2$, and 0.5 to $\chi^+\chi^-$ and $\tilde{\chi}_1\tilde{\chi}_1$. The maximum value of $\sigma \times Br$ is 0.01 pb, occurring at $m_{H_2} = 291$ GeV, $m_{\tilde{\chi}_1} \approx m_{\tilde{\chi}_2} = 109$ GeV, $\sigma(gg \to H_2) \sim 0.13$ pb, and $Br(H_2 \to \tilde{\chi}_2\tilde{\chi}_1) \sim 0.1$. The relevant decay branching ratios of H_2 were also presented.

The results obtained from the analysis of the DPS-N2HDM and NUH-NMSSM parameter spaces showed the accommodated values of the production of a non-SM-like H_2 via gluon fusion and its subsequent decay into DM particles. However, the DPS-N2HDM allowed for higher production cross-sections than the NUH-NMSSM, with the maximum value of $Br \times \sigma$ found in the DPS-N2HDM being larger than that in the NUH-NMSSM. Moreover, the allowed parameter space in the DPS-N2HDM showed that the branching ratio $Br(H_2 \to H_D H_D)$ reaches values close to 100%, especially for regions where the mass of the dark singlet is below 200 GeV. On the other hand, the NUH-NMSSM parameter space allowed for quasi-invisible decays where the LSP and NLSP are mass-degenerate. In both models, the relic density was found to be below the lower bound, indicating that this parameter space can partially explain dark matter. And while the DM particle is an SM-singlet scalar in the DSP-N2HDM, it was mostly Higgsino in the scanned parameter space of the NUH-NMSSM. It is worth emphasizing that in the MSSM, the parameter space with Higgsino-like DM is largely restricted compared with the NMSSM. Indeed, it was shown in Ellis et al. (2023) that the viable regions of the constrained MSSM parameter space allow for Higgsino DM with a mass ranging from 1 TeV to 1.1 TeV.

In conclusion, we showed that the DSP-N2HDM and NUH-NMSSM can pass all recent experimental constraints while providing challenging scenarios for collider searches of extended Higgs sectors, focusing particularly on a non-SM-like H_2. We also showed that the predictions of these models for the invisible decay of H_2 to dark matter particles are quite different, indicating a possible way to distinguish both models. We made no assumptions regarding the relationship between the N2HDM and the NMSSM, which can be the subject of a future study.

Declaration of competing interest

I declare no conflicts of interests.

Acknowledgment

MB acknowledges support from the King Saud University Deanship of Scientific Research.

References

Aad, Georges, et al., 2012. Observation of a new particle in the search for the standard model Higgs boson with the ATLAS detector at the LHC. Phys. Lett. B 716, 1–29.

Adhikary, Amit, Barman, Rahool Kumar, Bhattacherjee, Biplob, De, Amandip, Godbole, Rohini M., Kulkarni, Suchita, 2023. Long-lived NLSP in the NMSSM. Phys. Rev. D 108, 035020.

Ananthanarayan, B., Lahiri, Jayita, Pandita, P.N., 2015. Invisible decays of the heavier Higgs boson in the minimal supersymmetric standard model. Phys. Rev. D 91, 115025.

ATLAS Collaboration, 2022. A detailed map of Higgs boson interactions by the ATLAS experiment ten years after the discovery. Nature 607 (7917), 52–59; Erratum:, 2022. Nature 612, E24.

Azevedo, Duarte, Ferreira, Pedro, Margarete Mühlleitner, M., Santos, Rui, Wittbrodt, Jonas, 2019. Models with extended Higgs sectors at future e^+e^- colliders. Phys. Rev. D 99 (5), 055013.

Baum, Sebastian, Shah, Nausheen R., Freese, Katherine, 2019. The NMSSM is within reach of the LHC: Mass correlations & decay signatures. J. High Energy Phys. 04, 011.

Bechtle, Philip, Dercks, Daniel, Heinemeyer, Sven, Klingl, Tobias, Stefaniak, Tim, Weiglein, Georg, Wittbrodt, Jonas, 2020. HiggsBounds-5: Testing Higgs sectors in the LHC 13 TeV era. Eur. Phys. J. C 80 (12), 1211.

Bechtle, Philip, Heinemeyer, Sven, Klingl, Tobias, Stefaniak, Tim, Weiglein, Georg, Wittbrodt, Jonas, 2021. HiggsSignals-2: Probing new physics with precision Higgs measurements in the LHC 13 TeV era. Eur. Phys. J. C 81 (2), 145.

Belanger, Genevieve, Mjallal, Ali, Pukhov, Alexander, 2021. Recasting direct detection limits within micrOMEGAs and implication for non-standard dark matter scenarios. Eur. Phys. J. C 81 (3), 239.

Biekötter, Thomas, Grohsjean, Alexander, Heinemeyer, Sven, Schwanenberger, Christian, Weiglein, Georg, 2022. Possible indications for new Higgs bosons in the reach of the LHC: N2HDM and NMSSM interpretations. Eur. Phys. J. C 82 (2), 178.

Cao, Junjie, Jia, Xinglong, Meng, Lei, Yue, Yuanfang, Zhang, Di, 2023. Status of the singlino-dominated dark matter in general next-to-minimal supersymmetric standard model. J. High Energy Phys. 03, 198.

CERN Yellow Report, 0000. Bsm Higgs production cross sections at 13 tev (update in cern report4 2016).

Chatrchyan, Serguei, et al., 2012. Observation of a new boson at a mass of 125 GeV with the CMS experiment at the LHC. Phys. Lett. B 716, 30–61.

Chen, Chien-Yi, Freid, Michael, Sher, Marc, 2014. Next-to-minimal two Higgs doublet model. Phys. Rev. D 89 (7), 075009.

Das, Debottam, Ellwanger, Ulrich, Teixeira, Ana M., 2012. NMSDECAY: A fortran code for supersymmetric particle decays in the next-to-minimal supersymmetric standard model. Comput. Phys. Comm. 183, 774–779.

Domingo, Florian, Ellwanger, Ulrich, Hugonie, Cyril, 2022. M_W, Dark matter and a_μ in the NMSSM. Eur. Phys. J. C 82 (11), 1074.

Drozd, Aleksandra, Grzadkowski, Bohdan, Gunion, John F., Jiang, Yun, 2014. Extending two-Higgs-doublet models by a singlet scalar field - the case for dark matter. J. High Energy Phys. 11, 105.

Dutta, Juhi, Moortgat-Pick, Gudrid, Schreiber, Merle, 2022. Phenomenology of the dark matter sector in the two Higgs doublet model with complex scalar singlet extension. PoS 265, 3, ICHEP2022.

Ellis, John, Olive, Keith A., Spanos, Vassilis C., Stamou, Ioanna D., 2023. The CMSSM survives Planck, the LHC, LUX-ZEPLIN, Fermi-LAT, H.E.S.S. and IceCube. Eur. Phys. J. C 83 (3), 246.

Ellwanger, Ulrich, Gunion, John F., Hugonie, Cyril, 2005. NMHDECAY: A Fortran code for the Higgs masses, couplings and decay widths in the NMSSM. J. High Energy Phys. 02, 066.

Ellwanger, Ulrich, Hugonie, Cyril, 2006. NMHDECAY 2.0: An updated program for sparticle masses, Higgs masses, couplings and decay widths in the NMSSM. Comput. Phys. Comm. 175, 290–303.

Ellwanger, Ulrich, Hugonie, Cyril, 2012. Higgs bosons near 125 GeV in the NMSSM with constraints at the GUT scale. Adv. High Energy Phys. 2012, 625389.

Ellwanger, Ulrich, Hugonie, Cyril, 2022. Benchmark planes for Higgs-to-Higgs decays in the NMSSM. Eur. Phys. J. C 82 (5), 406.

Ellwanger, Ulrich, Hugonie, Cyril, Teixeira, Ana M., 2010. The next-to-minimal supersymmetric standard model. Phys. Rep. 496, 1–77.

Ellwanger, Ulrich, Teixeira, Ana M., 2014. NMSSM with a singlino LSP: possible challenges for searches for supersymmetry at the LHC. J. High Energy Phys. 10, 113.

Ellwanger, et al., 0000. NMSSMTOOLS - Home, https://www.lupm.univ-montp2.fr/users/nmssm/index.html.

Engeln, Isabell, Mühlleitner, Margarete, Wittbrodt, Jonas, 2019. N2HDECAY: Higgs Boson decays in the different phases of the N2HDM. Comput. Phys. Comm. 234, 256–262.

Harlander, Robert V., Liebler, Stefan, Mantler, Hendrik, 2017. SusHi Bento: Beyond NNLO and the heavy-top limit. Comput. Phys. Comm. 212, 239–257.

King, S.F., Mühlleitner, M., Nevzorov, R., Walz, K., 2014. Discovery prospects for NMSSM Higgs bosons at the high-energy large hadron collider. Phys. Rev. D 90 (9), 095014.

Miller, D.J., Nevzorov, R., Zerwas, P.M., 2004. The Higgs sector of the next-to-minimal supersymmetric standard model. Nuclear Phys. B 681, 3–30.

Mühlleitner, Margarete, Sampaio, Marco O.P., Santos, Rui, Wittbrodt, Jonas, 2017a. The n2hdm under theoretical and experimental scrutiny. J. High Energy Phys. 2017 (3).

Mühlleitner, Margarete, Sampaio, Marco O.P., Santos, Rui, Wittbrodt, Jonas, 2017b. Phenomenological comparison of models with extended Higgs sectors. J. High Energy Phys. 08, 132.

Mühlleitner, Margarete, Sampaio, Marco O.P., Santos, Rui, Wittbrodt, Jonas, 2022. ScannerS: parameter scans in extended scalar sectors. Eur. Phys. J. C 82 (3), 198.

Peccei, R.D., Quinn, Helen R., 1977a. Constraints imposed by CP conservation in the presence of pseudoparticles. Phys. Rev. D 16, 1791–1797.

Peccei, R.D., Quinn, Helen R., 1977b. CP Conservation in the presence of pseudoparticles. Phys. Rev. Lett. 38, 1440–1443.

Telba, Marwa, Binjonaid, Maien, 2021a. Fermionic decays of NMSSM Higgs bosons under LHC 13 TeV constraints. Results Phys. 27, 104464.

Telba, Marwa, Binjonaid, Maien, 2021b. Impact of LHC Higgs couplings measurements on bosonic decays of the neutral Higgs sector in the scNMSSM. Modern Phys. Lett. A 36 (06), 2150035.

Tumasyan, Armen, et al., 2022. A portrait of the Higgs boson by the CMS experiment ten years after the discovery. Nature 607 (7917), 60–68.

Wang, Kun, Zhu, Jingya, 2020a. Funnel annihilations of light dark matter and the invisible decay of the Higgs boson. Phys. Rev. D 101 (9), 095028.

Wang, Kun, Zhu, Jingya, 2020b. A novel scenario in the semi-constrained NMSSM. J. High Energy Phys. 06, 078.